Supporting information

A synergistic architecture design on integrally boosting the hydroxyl adsorption and charge transfer for oxygen evolution reaction

Jiani Chen, [a†] Shiliang Zhu, [a†] Lei Ge, [b] Sixuan She, [c] Dongliang Liu, [a] Yuchen Sha, [a] Wei Zhou, *[a] and Zongping Shao *[ad]

[a] State Key Laboratory of Materials-Oriented Chemical Engineering, College of Chemical Engineering, Nanjing Tech University, Nanjing, China.
[b] Centre for Future Materials, University of Southern Queensland, Springfield Central, QLD 4300, Australia.
[c] Department of Applied Physics, The Hong Kong Polytechnic University, Hung Hom, Kowloon, Hong Kong, China.
[d] WA School of Mines: Minerals, Energy and Chemical Engineering (WASM-MECE), Curtin University, Perth, Western Australia, Australia.
† The authors contributed equally to this work.

Experimental Section

Catalyst preparation

$Pr_{0.5}Ba_{0.25}Sr_{0.25}Co_{0.8}Fe_{0.2}O_{3-\delta}$ (denote as $Pr_{0.5}$BSCF) was synthesized using a standard combined EDTA-citrate complexing sol-gel method. Typically, stoichiometric amounts of $Pr(NO_3)_3 \cdot 6H_2O$, $Ba(NO_3)_2$, $Sr(NO_3)_2$, $Co(NO_3)_2 \cdot 6H_2O$ and $Fe(NO_3)_3 \cdot 9H_2O$ (all are the analytical grade, Sinopharm Chemical Reagent Co., Ltd.) were completely dissolved in deionized water. Citrate ($C_{10}H_{16}N_2O_8$, Sinopharm Chemical Reagent Co., Ltd.) and EDTA ($C_6H_8O_7$, Sinopharm Chemical Reagent Co., Ltd.) were introduced to the above solution at a molar ratio of 2:1:1 for citrate/EDTA/metal ions and then an aqueous ammonium hydroxide solution (NH_3, 28%, Sinopharm Chemical Reagent Co., Ltd.) was also added until the solution pH reached 6. The obtained transparent solution was heated at 90 ^oC with continuous stirring to achieve a gel and pre-treated at 250 ^oC for 5 h to form a solid precursor. The precursor was finally calcined at 1100 ^oC for 5 h in air to obtain the final product.

The $Pr_{0.5}$-Co_3O_4 was prepared by a modified molten-salt method.[1] Briefly, 0.02 g of CoO (Aladdin Industrial Corporation.), 0.1 g of $Pr_{0.5}$BSCF, 0.11 g of KCl and 0.09 g of LiCl were thoroughly ground in a mortar. The homogenous mixture was transferred into a tube furnace and calcined at 500 ^oC for 2 h under Ar atmosphere. After cooling down naturally, the mixture was washed with water several times to remove the salt (KCl and LiCl) and then dried at 60 ^oC to obtain the product.

The $Pr_{0.5}$-MS was prepared by the same method as $Pr_{0.5}$-Co_3O_4, excepting no CoO was added. CoO was also treated with the molten-salt method to prepare Co_3O_4, which acted as the reference sample during XPS analysis.

To prepare the control samples $Pr_{0.5}$+Co_3O_4 and $Pr_{0.5}$-MS+Co_3O_4, the stoichiometric amounts of Co_3O_4 were added in a mortar and finely ground with $Pr_{0.5}$BSCF and $Pr_{0.5}$-MS, respectively for at least 30 min.

Materials characterization

The phase structures were characterized by powder X-ray diffraction (XRD, Rigaku Smartlab 3kW) equipped with filtered Cu Kα radiation (λ = 1.5406 Å, 40 kV, 40 mA). XRD Rietveld refinement was conducted using the GSAS-EXPGUI package. The morphologies and microstructures were analyzed by scanning electron microscope (SEM, Hitachi S-4800) and transmission electron microscope (TEM, JEM-2100). The BET surface area was measured by nitrogen adsorption-desorption isotherms (BELSORP II). The element chemical states on the catalyst surface were determined by X-ray photoelectron spectroscopy (XPS, PHI 5000 VersaProbe) equipped with an Al Kα X-ray source. The element spectra were fitted by the XPS Peak software with C 1s peak calibrated to 284.8 eV. TG data was collected by a thermobalance (STA 449 F3 Jupiter). Raman spectroscopy was performed on a Horiba LabRAM HR Evolution Raman technique.

Electrochemical measurements

Working electrodes of samples were prepared by a controlled drop-casting method. Specifically, the catalyst ink was prepared by sufficiently sonicating a mixture of 10 mg of catalyst, 10 mg of Super P Li and 0.1 mL of 5 wt% Nafion solution dispersed in 1 mL of

absolute ethanol. Afterwards, the 5 μL of homogenous catalyst ink was transferred onto the polished glassy carbon electrodes (GC, 0.196 cm^2, Pine Research Instrumentation).
Electrochemical measurements were conducted with a typical three-electrode electrochemical cell (Pine Research Instrumentation) with an RDE set-up controlled by an electrochemical workstation (CHI 760E). Ag/AgCl (3.5 M KCl) and graphite rod were used as the reference and counter electrode, respectively. The 0.1 M KOH electrolyte was bubbled with O_2 for at least 0.5 h to ensure O_2-saturated for the O_2/H_2O equilibrium at 1.23 V vs. RHE. Polarization curves were collected at a rotation rate of 1600 rpm with a scan rate of 5 mV s^{-1} from 0.2-1.0 V (vs. Ag/AgCl) range. Ohmic losses were compensated for the polarization curves with iR-corrected: $E = E_{exp} - iR$, in which E_{exp} is the experimental potential, i represents the tested current, and R is the solution resistance which is about 40 Ω. Electrochemical impedance spectroscopy (EIS) was performed from 0.1 Hz to 100000 Hz at 0.7 V (vs. Ag/AgCl) with the influence of an AC voltage of 10 mV. Cyclic voltammetry (CV) was applied to measure the electrochemical double-layer capacitance (C_{dl}). The potential was swept from 0.2 to 0.3 V (vs. Ag/AgCl) at different scan rates of 10, 20, 40, 60, 80, 100 and 120 mV s^{-1}. For the stability test, chronopotentiometry was executed under an anodic current density of 10 mA cm^{-2} on a carbon cloth with a loading of 1 mg cm^{-2}.

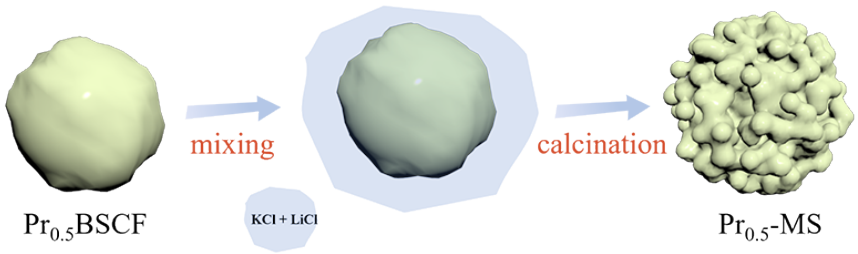

Figure S1. Illustration of molten-salt preparation of $Pr_{0.5}$-MS.

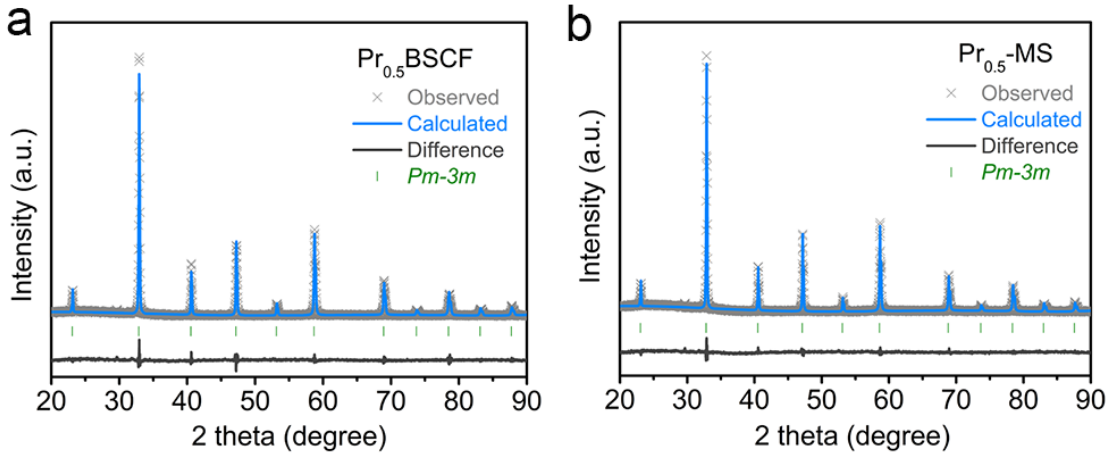

Figure S2. The XRD patterns and refinements of (a) $Pr_{0.5}$BSCF and (b) $Pr_{0.5}$-MS. The standard card number for *Pm-3m* sapce group is JCPDS No. 01-082-2445.

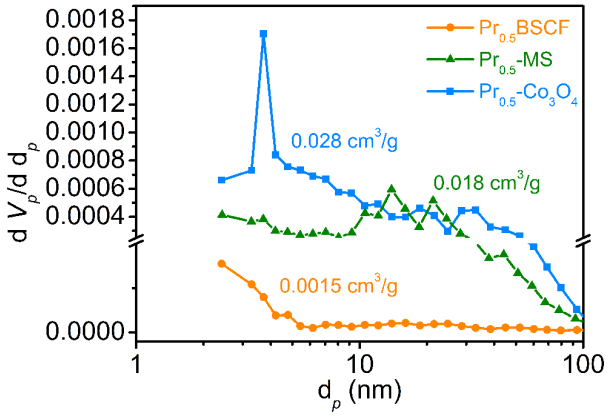

Figure S3. The corresponding Barrett-Joyner-Halenda (BJH) pore size distribution plots of catalysts.

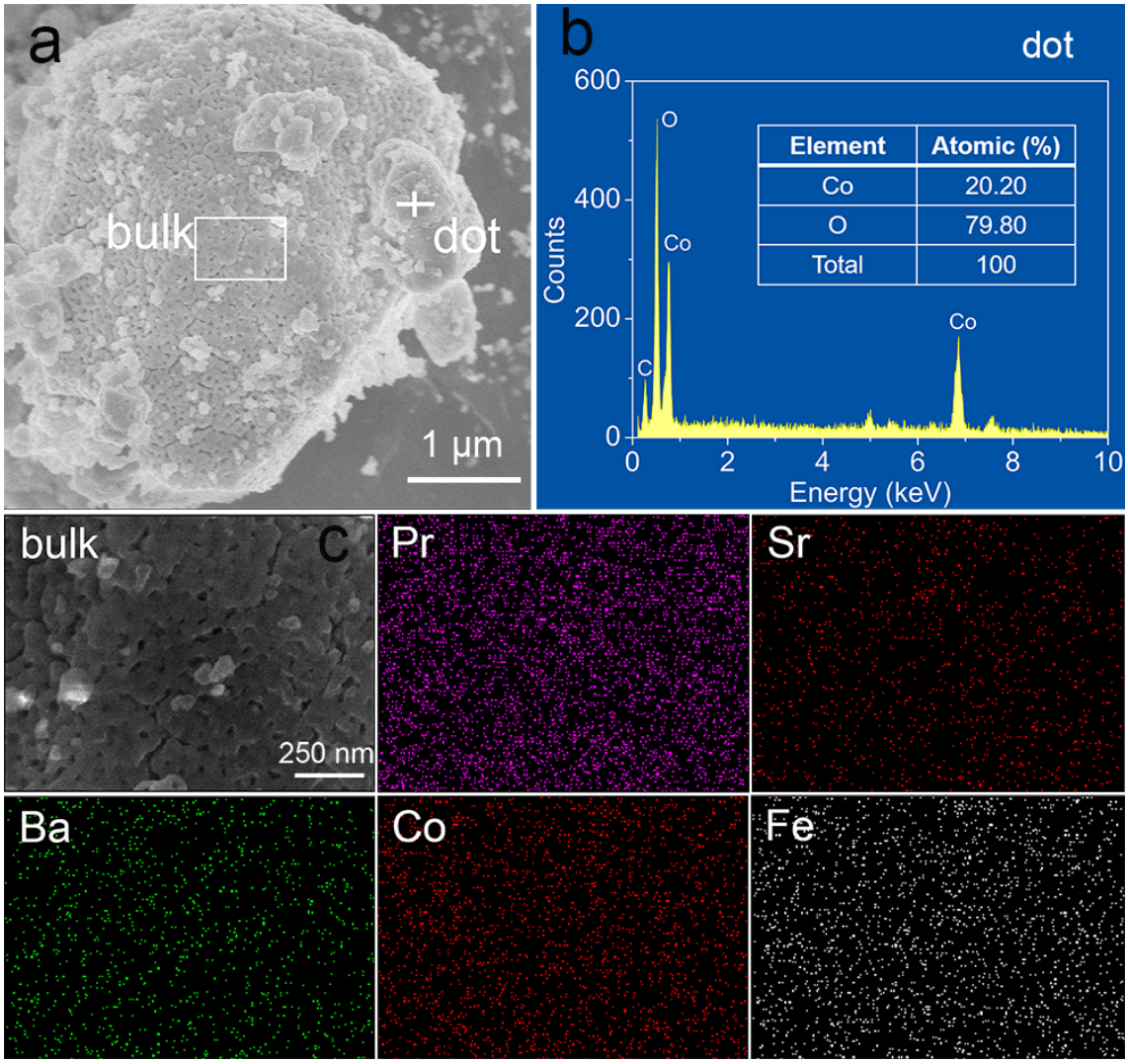

Figure S4. (a) SEM image, (b) point EDX scanning result, and (c) SEM-EDX result of $Pr_{0.5}$-Co_3O_4.

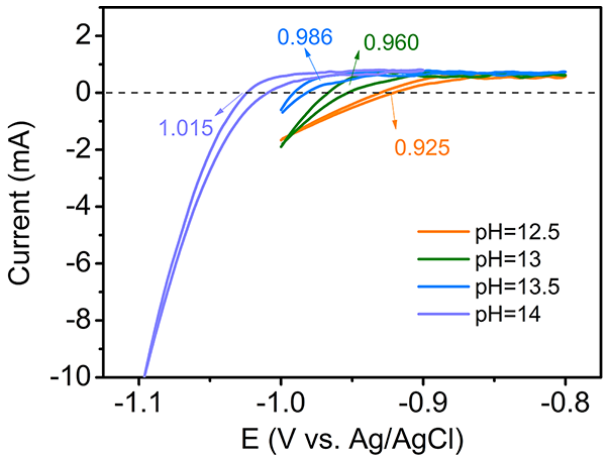

Figure S5. RHE calibration of Ag/AgCl reference electrode under different pH values.

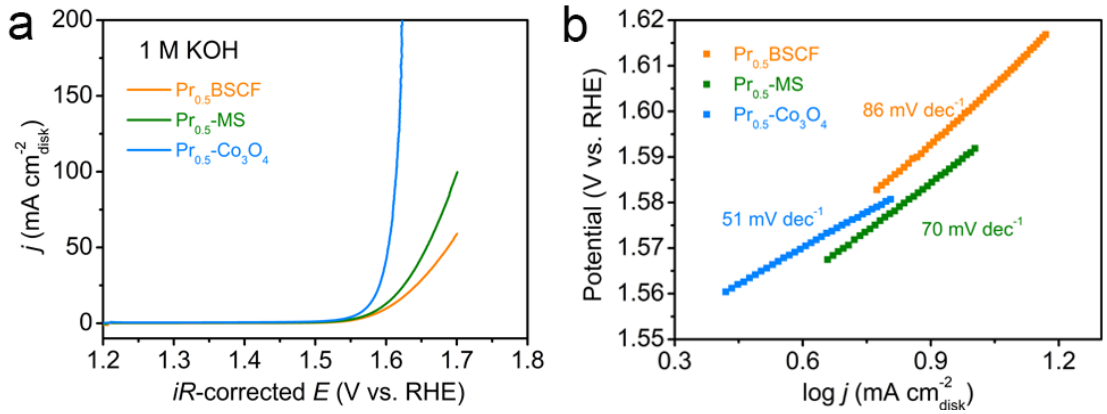

Figure S6. (a) Polarization curves and (b) Tafel slopes of $Pr_{0.5}$BSCF, $Pr_{0.5}$-MS and $Pr_{0.5}$-Co_3O_4 in 1 M KOH solution.

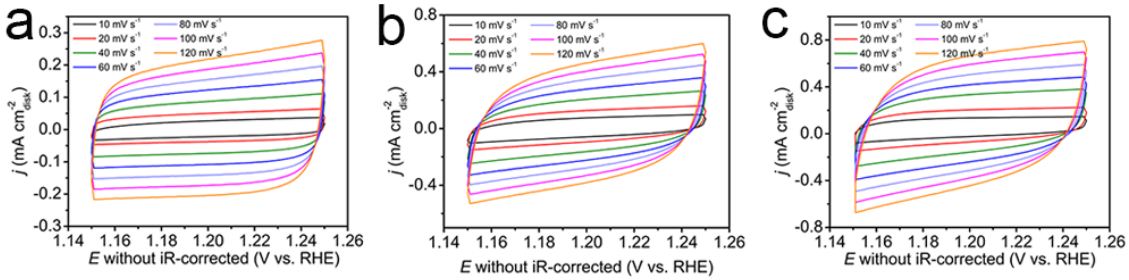

Figure S7. CV scans recorded for (a) $Pr_{0.5}$BSCF, (b) $Pr_{0.5}$-MS and (c) $Pr_{0.5}$-Co_3O_4 at different scan rates.

ECSA was reckoned by the non-faradic double layer capacitance (C_{dl}) method and calculated with the following equation: ECSA = C_{dl}/C_s, where C_s represents specific capacitance, and it is generally assumed that C_s of the oxide is 40 μF cm^{-2}.

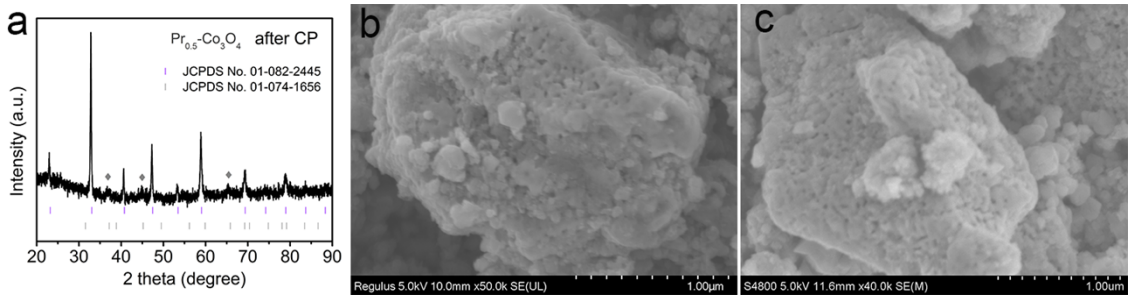

Figure S8. (a) XRD pattern of $Pr_{0.5}$-Co_3O_4 after longtime work. (b-c) SEM images of $Pr_{0.5}$-Co_3O_4 after longtime work.

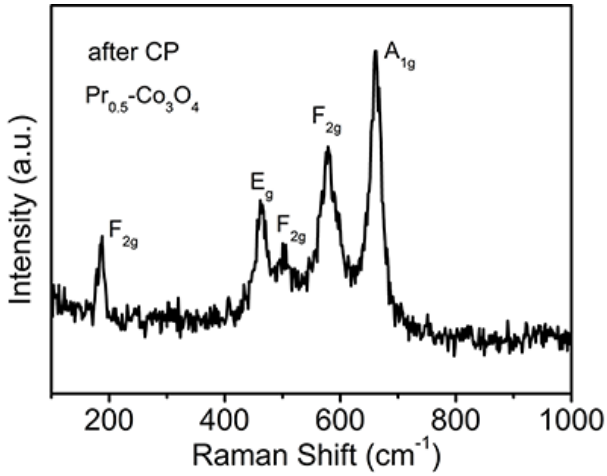

Figure S9. Raman spectra of $Pr_{0.5}$-Co_3O_4 after longtime work.

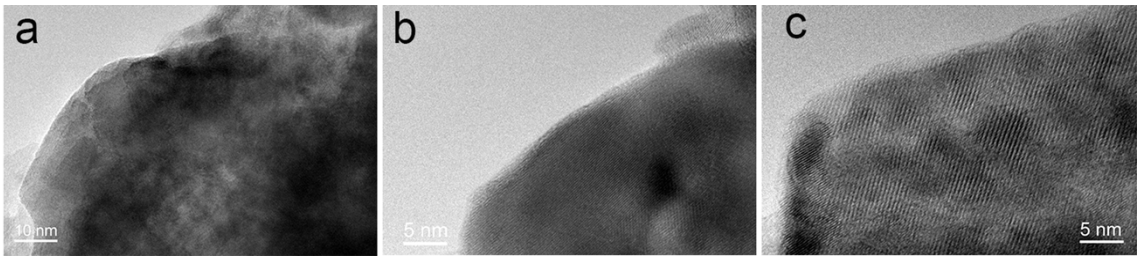

Figure S10. TEM images of $Pr_{0.5}$-Co_3O_4 after longtime work.

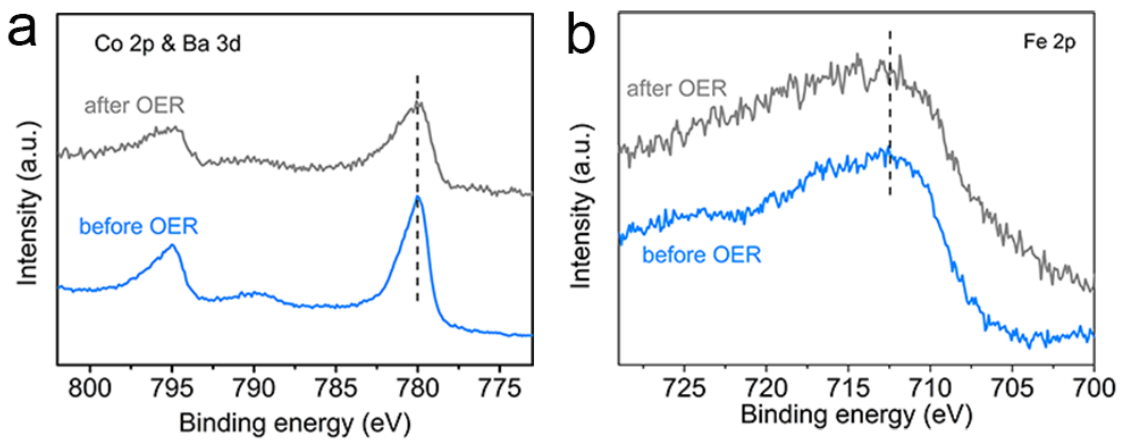

Figure S11. (a) Co 2p/Ba 3d XPS and (b) Fe 2p spectra of $Pr_{0.5}$-Co_3O_4 sample before and after longtime work.

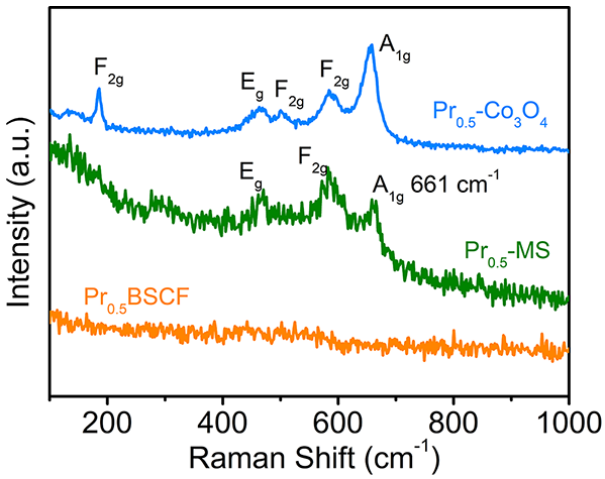

Figure S12. Raman spectra of $Pr_{0.5}$BSCF, $Pr_{0.5}$-MS and $Pr_{0.5}$-Co_3O_4.

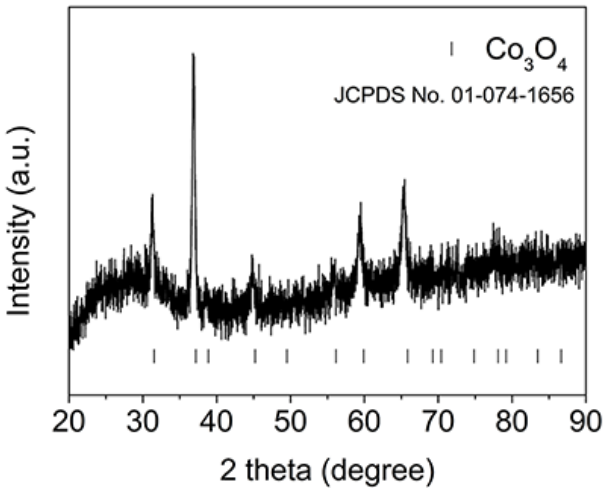

Figure S13. XRD pattern of Co_3O_4 which prepared with CoO via the molten-salt treatment.

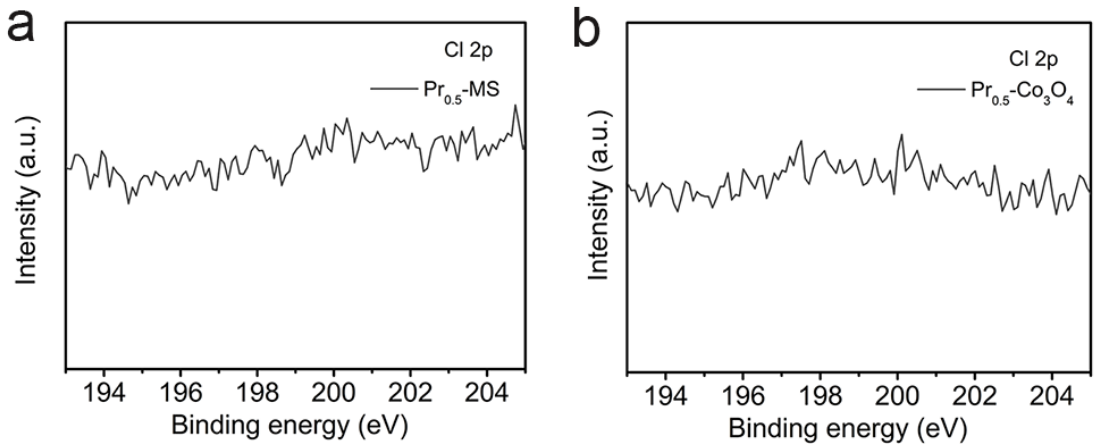

Figure S14. Cl 2p XPS spectra of (a) $Pr_{0.5}$-MS and (b) $Pr_{0.5}$-Co_3O_4.

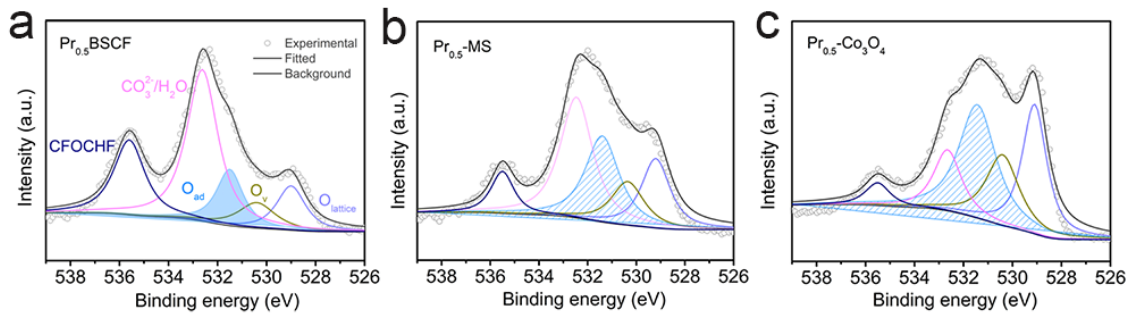

Figure S15. O 1s XPS spectra of (a) $Pr_{0.5}$BSCF, (b) $Pr_{0.5}$-MS, and (c) $Pr_{0.5}$-Co_3O_4 after OER. The peak at ~535.5 eV is originated from the CFOCHF of Nafion solution, which was introduced during electrode preparation.[2, 3]

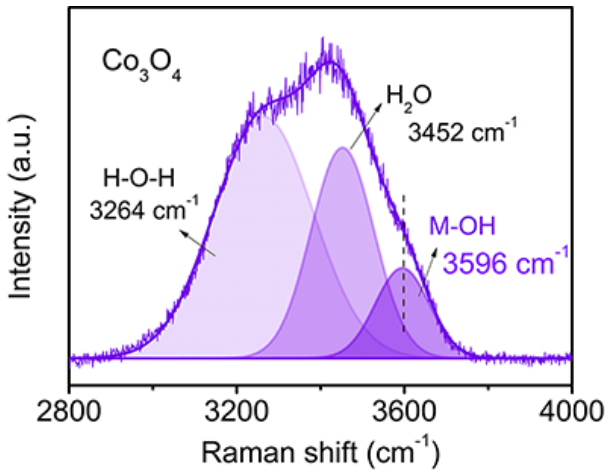

Figure S16. In situ Raman spectra of Co_3O_4 at 0.8 V vs Ag/AgCl.

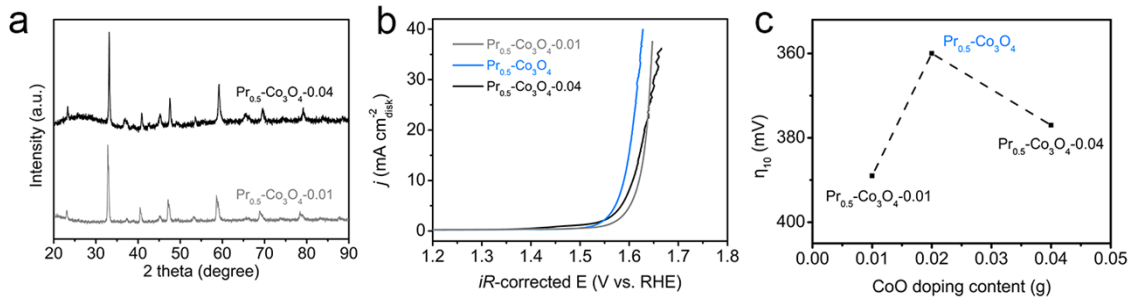

Figure S17. (a) XRD patterns of catalysts with different initial CoO doping content. The X in $Pr_{0.5}$-Co_3O_4-X represents the CoO doping content of 0.01g and 0.02g. (b) Polarization curves of three samples in 0.1 M KOH solution. (c) Oxygen evolution activity as a function of initial CoO doping content.

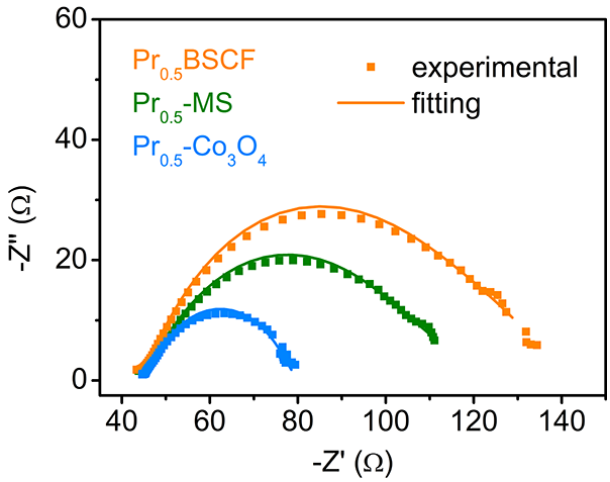

Figure S18. The EIS Nyquist plots for three catalysts. The configuration is R_s-(R_{p1}-CPE_1)-(R_{p2}-CPE_2), in which R_s represents the ohmic resistance of electrolyte, while CPE_1 and CPE_2 are constant phase parameters.

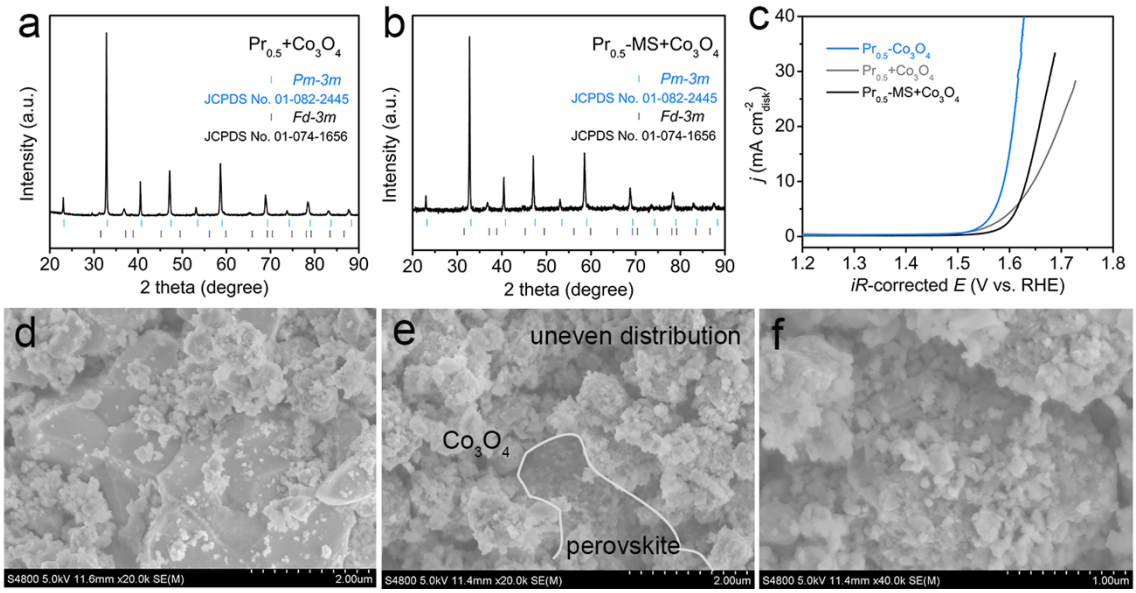

Figure S19. XRD patterns of control samples (a)$Pr_{0.5}$+Co_3O_4 and (b) $Pr_{0.5}$-MS+Co_3O_4 fabricated by physical mixing. (c) Polarization curves of samples in 0.1 M KOH solution. SEM images of (d)$Pr_{0.5}$+Co_3O_4, (e) and (f) $Pr_{0.5}$-MS+Co_3O_4.

Table S1. XRD Rietveld refinement judgmental parameters of three samples.

Catalysts	R_{wp}(%)	R_p(%)	R_{exp}(%)	GOF
$Pr_{0.5}$BSCF	5.37	4.25	3.48	1.46
$Pr_{0.5}$-MS	5.38	4.31	3.46	1.45
$Pr_{0.5}$-Co_3O_4	3.9	2.92	2.82	1.38

Table S2. Tafel slopes and overpotential required to achieve a current density of 10 mA cm^{-2} for the related OER catalysts.

Catalysts	Electrolyte	η_{10} (mV)	Tafel slope (mV dec^{-1})	Reference
$Pr_{0.5}$-Co_3O_4	**0.1 M KOH**	**360**	**58**	**This work**
	1 M KOH	**342**	**51**	
$PrBa_{0.5}Sr_{0.5}Co_{1.5}Fe_{0.5}O_{5+\delta}$-III	0.1 M KOH	358	52	Ref[4]
$PrBa_{0.5}Sr_{0.5}Co_{1.5}Fe_{0.5}O_{5+\delta}$ film	1 M KOH	460	94	Ref[5]
$PrBaCo_2O_{5.75}$	1 M KOH	360	70	Ref[6]
$Ba_{0.5}Sr_{0.5}Co_{0.8}Fe_{0.2}O_{3-\delta}$	0.1 M KOH	490	84	Ref[7]
$LaSr_3Co_{1.5}Fe_{1.5}O_{10-\delta}$	0.1 M KOH	388	84	Ref[8]
$Ba_{0.35}Sr_{0.65}Co_{0.8}Fe_{0.2}O_{3-\delta}$	0.1 M KOH	260	N.A.	Ref[9]
Co_3O_4 nanotubes	1 M KOH	390	76	Ref[10]
$Co_3O_{3.87}F_{0.13}$	0.1 M KOH	430	56	Ref[11]
V-$LaCoO_{3-\delta}$/Co_3O_4	1 M KOH	354	73	Ref[12]
Co_3O_4/Co-Fe oxide	1 M KOH	297	61	Ref[13]
Co_3O_4/$La_{0.3}Sr_{0.7}CoO_3$	0.1 M KOH	380	75	Ref[14]

N.A. = Not available.

Table S3a. The relative amounts of the four different surface oxygen species of three samples before OER.

Catalysts	$O_{lattice}$ (%)	O_2^{2-}/O^-(%)	OH^-/O_2(%)	H_2O(%)
$Pr_{0.5}$BSCF	22.1	19.0	53.2	5.7
$Pr_{0.5}$-MS	32.9	10.1	44.5	12.5
$Pr_{0.5}$-Co_3O_4	43.6	13.3	34.1	9.0

Table S3b. The relative amounts of the four different surface oxygen species of three samples after OER.

Catalysts	$O_{lattice}$ (%)	O_2^{2-}/O^-(%)	OH^-/O_2(%)	H_2O(%)
$Pr_{0.5}$BSCF	15.2	11.2	17.8	55.8
$Pr_{0.5}$-MS	19.4	13.9	28.4	38.3
$Pr_{0.5}$-Co_3O_4	28.4	20.7	35.8	15.1

The content of CHFCFO was excluded for the convenient comparison with the sample states before OER.

1 M. Xiao, L. Zhang, B. Luo, M. Lyu, Z. Wang, H. Huang, S. Wang, A. Du and L. Wang, *Angew. Chem., Int. Ed.*, 2020, **59**, 7230–7234.

2 Y. Zhu, H. A. Tahini, Y. Wang, Q. Lin, Y. Liang, C. M. Doherty, Y. Liu, X. Li, J. Lu, S. C. Smith, C. Selomulya, X. Zhang, Z. Shao and H. Wang, *J. Mater. Chem. A*, 2019, **7**, 14222–14232.

3 B. Tazi and O. Savadogo, *Electrochim. Acta*, 2000, **45**, 4329–4339.

4 B. Zhao, L. Zhang, D. Zhen, S. Yoo, Y. Ding, D. Chen, Y. Chen, Q. Zhang, B. Doyle, X. Xiong and M. Liu, *Nat. Commun.*, 2017, **8**, 14586.

5 Y. Zhu, X. Zhong, S. Jin, H. Chen, Z. He, Q. Liu and Y. Chen, *J. Mater. Chem. A*, 2020, **8**, 10957–10965.

6 X. Miao, L. Wu, Y. Lin, X. Yuan, J. Zhao, W. Yan, S. Zhou and L. Shi, *Chem. Commun.*, 2019, **55**, 1442–1445.

7 C. Su, W. Wang, Y. Chen, G. Yang, X. Xu, M. O. Tade and Z. Shao, *ACS Appl. Mater. Interfaces*, 2015, **7**, 17663–17670.

8 S. Liu, H. Luo, Y. Li, Q. Liu and J.-L. Luo, *Nano Energy*, 2017, **40**, 115–121.

9 D. Guan, G. Ryu, Z. Hu, J. Zhou, C.-L. Dong, Y.-C. Huang, K. Zhang, Y. Zhong, A. C. Komarek, M. Zhu, X. Wu, C.-W. Pao, C.-K. Chang, H.-J. Lin, C.-T. Chen, W. Zhou and Z. Shao, *Nat. Commun.*, 2020, **11**, 3376.

10 H. Wang, S. Zhuo, Y. Liang, X. Han and B. Zhang, *Angew. Chem., Int. Ed.*, 2016, **55**, 9055–9059.

11 H. Zeng, M. h. Oubla, X. Zhong, N. Alonso-Vante, F. Du, Y. Xie, Y. Huang and J. Ma, *Appl. Catal. B Environ.*, 2021, **281**, 119535.

12 J. Zhang, J. Li, C. Zhong, P. Xi, D. Chao and D. Gao, *Nano Lett.*, 2021, **21**, 8166–8174.

13 X. Wang, L. Yu, B. Y. Guan, S. Song and X. W. D. Lou, *Adv. Mater.*, 2018, **30**, 1801211.

14 X. Wang, Z. Pan, X. Chu, K. Huang, Y. Cong, R. Cao, R. Sarangi, L. Li, G. Li and S. Feng, *Angew. Chem., Int. Ed.*, 2019, **58**, 11720–11725.